Acta Geochim (2025) 44:1340–1351
https://doi.org/10.1007/s11631-025-00814-6

ORIGINAL ARTICLE

Mercury isotope geochemistry of the Aketashi VMS deposit: Constraints on ore-forming fluid sources

Ziru Jin[1,2] · Zhengwei Zhang[1] · Chengquan Wu[1] · Jinhong Xu[1,3] · Xiyao Li[1]

Received: 13 March 2025 / Revised: 3 July 2025 / Accepted: 14 July 2025 / Published online: 27 August 2025

Abstract This study investigates the mercury (Hg) isotope geochemistry of pyrite from the Aketashi volcanic hosted massive sulfide (VMS) deposit in the West Kunlun Orogenic Belt, China, aiming to elucidate the sources of ore-forming fluids and the behavior of Hg isotopes during mineralization. The Aketashi deposit is located within a Late Paleozoic back-arc basin, which is characterized by extensive Carboniferous magmatism and hydrothermal activity. Analysis of 19 pyrite ore samples revealed Hg isotope composition with δ^{202}Hg values ranging from −2.48‰ to 0.87‰ and Δ^{199}Hg values from −0.02‰ to 0.40‰. The negative δ^{202}Hg values are indicative of isotopic fractionation resulting from hydrothermal processes, whereas the positive Δ^{199}Hg values imply a mixed fluid source comprising both magmatic and seawater-derived components. This study highlights the unique advantage of Hg isotopes in tracing multi-source fluid interactions (e.g., magmatic vs. seawater-derived) in VMS systems, providing a novel methodology for global metallogenic studies. Our findings not only resolve the long-standing debate on fluid origins at Aketashi but also establish a framework for applying Hg isotopes to other VMS deposits worldwide.

✉ Zhengwei Zhang
zhangzhengwei@vip.gyig.ac.cn

[1] State Key Laboratory of Critical Mineral Research and Exploration, Institute of Geochemistry, Chinese Academy of Sciences, Guanshanhu District, 99 West Lincheng Road, Guiyang 550081, China

[2] University of Chinese Academy of Sciences, Beijing 100039, China

[3] Institute of Resources and Environment, Tongren University, Tongren 554300, China

Keywords VMS deposits · Hg isotopes · West Kunlun · Ore-forming fluid sources

1 Introduction

Mercury is unique among metals in exhibiting both mass-dependent fractionation (MDF, expressed as δ^{202}Hg) and mass-independent fractionation (MIF, denoted as Δ^{199}Hg). Over the past decade, mercury isotope geochemistry has emerged as a powerful tool for tracing pollution sources in modern environments (Blum et al. 2014), reconstructing planetary formation processes (Meier et al. 2016) and identifying ancient catastrophic events such as volcanic eruptions and mass extinctions (Grasby et al. 2017; Shen et al. 2019; Thibodeau et al. 2016). Crucially, mercury isotopes are particularly effective in deciphering hydrothermal processes: MDF signatures track boiling, redox reactions, and mineral precipitation (Sherman et al. 2009; Smith et al. 2005, 2008), while MIF anomalies serve as robust tracers of fluid sources (Fu et al. 2020; Liu et al. 2021; Xu et al. 2018; Yin et al. 2019). These dual capabilities make mercury isotopes uniquely suited for tracing mineralization processes and material origins in hydrothermal systems (Xu et al. 2021). For instance, mercury isotopes can distinguish sedimentary-exhalative (SEDEX) and Mississippi Valley-type (MVT) deposits from magmatically influenced systems like volcanic-hosted massive sulfide (VMS) and intrusion-related (IR) deposits (Yin et al. 2016a). In addition, the combination of mercury isotopes with other isotopes, such as sulfur isotopes, serves as a valuable tool for elucidating the fluid sources and formation mechanisms of ore deposits (Wang et al. 2025; Zhang et al. 2025). However, systematic studies of mercury isotopes in VMS deposits remain scarce, particularly at the deposit scale, leaving their isotopic

variability and implications for metallogenic processes poorly constrained.

Volcanic-hosted massive sulfide (VMS) deposits represent critical global sources of base metals (e.g., Cu, Zn, Pb) and are natural laboratories for studying fluid–rock interactions (Barrie and Hannington 1997; Large et al. 2001). Their genesis involves complex processes, including magmatic degassing, seawater circulation, and hydrothermal alteration of host rocks (Hannington 2014). Despite decades of research, the relative contributions of magmatic versus sedimentary metal sources remain contentious. Traditional tracers (e.g., Pb isotopes, fluid inclusions) often lack diagnostic resolution to disentangle these components (Hannington et al. 2005). Mercury isotopes offer distinct advantages: (1) The high mobility of mercury in geothermal environments, its presence as Hg^0 in hydrothermal systems, and the dominance of Hg^0 under high-temperature reducing conditions render mercury isotopes valuable tracers for studying ore deposits (Varekamp and Buseck 1984; Zhao et al. 2023). (2) Mercury is a redox-sensitive, highly volatile chalcophile metal that exhibits pronounced geochemical similarities to Cu during magmatic and hydrothermal processes. It tends to be enriched in sulfide minerals, such as pyrite, chalcopyrite, and sphalerite, thereby directly capturing ore-forming signals (Rytuba 2003); (3) MIF anomalies ($\Delta^{199}Hg$) are sensitive to photochemical processes, providing fingerprints of near-surface fluid interactions (Smith et al. 2005; Yin et al. 2016a). Nonetheless, the behavior of mercury isotopes during VMS mineralization and their relationships to fluid sources are still enigmatic, partly due to the scarcity of deposit-scale isotopic datasets.

The Western Kunlun Orogen in China hosts significant VMS deposits but remains understudied due to its remote and rugged terrain. Previous work by Jia et al. (1999) and Mu (2016) established basic geological frameworks for regional sulfide deposits, yet the origin of ore-forming fluids remains unresolved. Here, we present the first mercury isotope analysis of pyrite from the Aketashi VMS deposit. Our objectives are threefold: (1) to characterize mercury isotope fractionation (MDF and MIF) during VMS mineralization; (2) to quantify contributions from potential fluid sources (magmatic, seawater-derived); and (3) to develop a mercury isotope-based model for tracing metal origins in VMS systems. This work not only advances understanding of the Aketashi deposit but also establishes mercury isotopes as a novel tracer for VMS metallogeny globally.

2 Geological background

The Western Kunlun Orogenic Belt, located in the westernmost part of China, originated from the prolonged tectonic evolution of the Tethyan Ocean (Fig. 1a; Pan 1990; Xiao et al. 2005; Zhang et al. 2007). It can be divided from south to north into the Karakoram Terrane, the West Kunlun Block, and the Southern Tarim Block (Fig. 1b). The Karakoram Terrane, situated on the northwest margin of the Tibetan Plateau, is considered a westward extension of the Qiangtang Terrane (Fig. 1a; Yin and Harrison 2000). The West Kunlun Block formed through the aggregation of several microcontinents during the Early Paleozoic (Cui et al. 2006) and is bounded by the Mazha-Kangxiwa mélange belt to the south (Li et al. 2007; 2006) and the Kegang fault zone to the north. The Southern Tarim Block, an active fault zone, was connected to the West Kunlun Block via the Tiekelike uplift during the Early Paleozoic (Mattern and Schneider 2000).

In the Late Paleozoic, the convergence of the Paleo-Tethys led to the formation of volcanic arcs and tectonic mélanges in the southern part of the West Kunlun Block (Li et al. 2007). This likely triggered the formation of the Oytag-Kuerliang back-arc basin in northern West Kunlun due to slab rollback (Liu et al. 2014b; Zhang et al. 2021). The Oytag-Kuerliang Basin underwent extensive and intense Carboniferous-Permian magmatism, marked by bimodal volcanism that resulted in the formation of the Wuluate Formation and the Keziliqiman Formation. Seafloor volcanism in the basin also led to intense hydrothermal activity, resulting in numerous VMS deposits, such as the Aketashi, Saluoyi, Shangqihan, and Tamuqi deposits (Wang et al. 2010; Song et al. 2021; Zhai et al. 2013). The Aketashi deposit is hosted in the Early Permian Keziliqiman Formation. This tectonic setting facilitated fluid mixing between magmatic-derived Cu–Zn-rich fluids and seawater. And during the Indosinian period, the Oytag-Kuerliang basin closed, causing regional uplift (Zhang et al. 2024).

3 Deposit geology

The Aketashi region lies in the northern part of the Oytag-Kuerliang Late Paleozoic back-arc basin, at the southwest margin of the Tarim Block (Fig. 2a). Over 20 VMS deposits, including Aketashi, Saluoyi, and Aketamu, have been identified in this region. Among them, the Aketashi VMS Cu–Zn deposit in the Kungai mountain in the northern area is the most representative (Fig. 2b; Jia et al. 1999).

The sedimentary sequence in the region comprises the Proterozoic Jixian Formation (Jxbc), the Late Carboniferous-Early Permian Tahaqi Formation (C_2P_1th), the Early Permian Keziliqiman Formation (P_1k), and the Quaternary (Q) (Jia et al. 1999; Sun 2003). The ore-bearing stratum is mainly the Keziliqiman Formation, which is predominantly composed of basalt, rhyolite, and rhyolitic tuff, with minor occurrences of limestone and metamorphic sandstone. The Keziliqiman Formation can be further subdivided into four distinct lithological units. The first unit is primarily

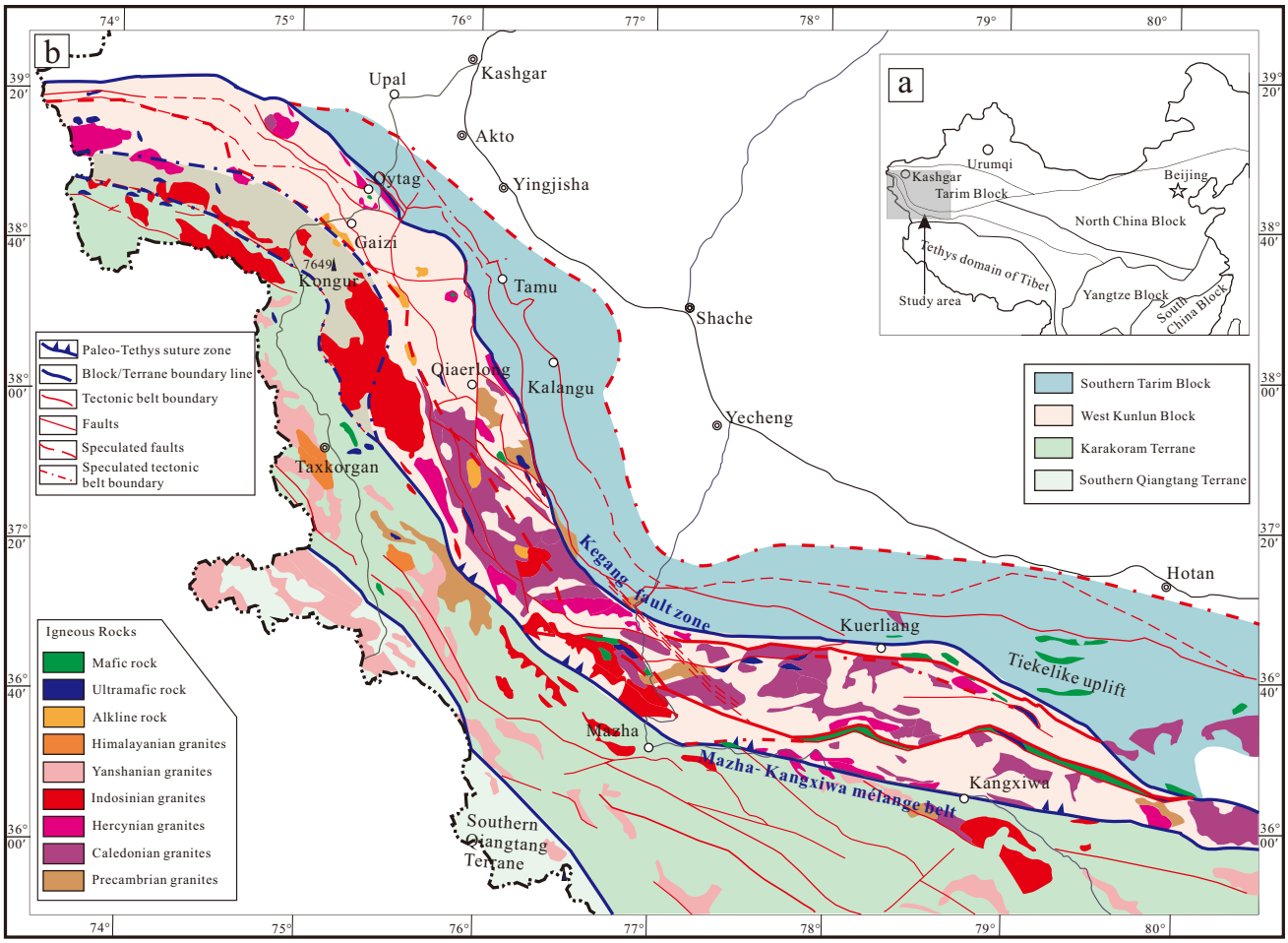

Fig. 1 Map showing the tectonic configuration of China (**a**) and distribution of tectonic framework in West Kunlun (**b**)

characterized by metamorphic sandstone and limestone. The second unit consists of tuff and spilite that have experienced extensive metamorphism. The third unit serves as the ore-hosting section, mainly comprising basalt. Most of the basalt has undergone metamorphism, forming sericite quartz-schist and chlorite-quartz schist. The contact between the fourth unit and the third unit is abrupt, marked by keratophyre and marble (Fig. 3).

The Aketashi deposit is divided into east, middle, and west ore sections, each containing 2–3 orebodies. They range in length from 300 to 1600 m and in thickness from 1 to 10 m. These stratiform orebodies are hosted in the meta-basalt of the third unit of the Keziliqiman Formation. The internal structure of the orebody is well-defined, exhibiting a clearly discernible double-layer characteristic. The upper layer consists of a massive sulfide ore zone, whereas the lower layer comprises a laminated sulfide ore zone. The meta-basalt is bounded by a sequence of thin-bedded marine carbonate rocks at both its top and bottom, suggesting that volcanic activity and mineralization processes took place within a marine environment (Fig. 4; Mu 2016). The mineralization likely formed through hydrothermal overprinting on pre-existing volcanic rocks, with the laminated ores predating the massive ores based on local intrusive relationships (Fig. 5a).

The laminated ores are dark gray to golden (Fig. 5b) and primarily composed of quartz, chlorite, muscovite, and abundant pyrite, with minor chalcopyrite. These minerals are well oriented, forming laminated structures. The pyrite grains are euhedral and medium-grained (0.2–1.0 mm in diameter), deformed and elongated along schistosity (Fig. 5c). The gangue minerals (quartz, chlorite, and muscovite) are similar to those in barren volcanic rocks.

In contrast, the massive ores are golden and lack distinct structures (Fig. 5d). They are dominated by sulfides, including pyrite (60%–70%), chalcopyrite (10%–15%), and sphalerite (5%–10%). Gangue minerals are minimal, mainly quartz with minor chlorite and carbonates. Pyrite grains in the massive ores are euhedral and medium-grained (0.2–1.2 mm in diameter), pure, smooth, and free of compositional zoning or inclusions (Fig. 5e).

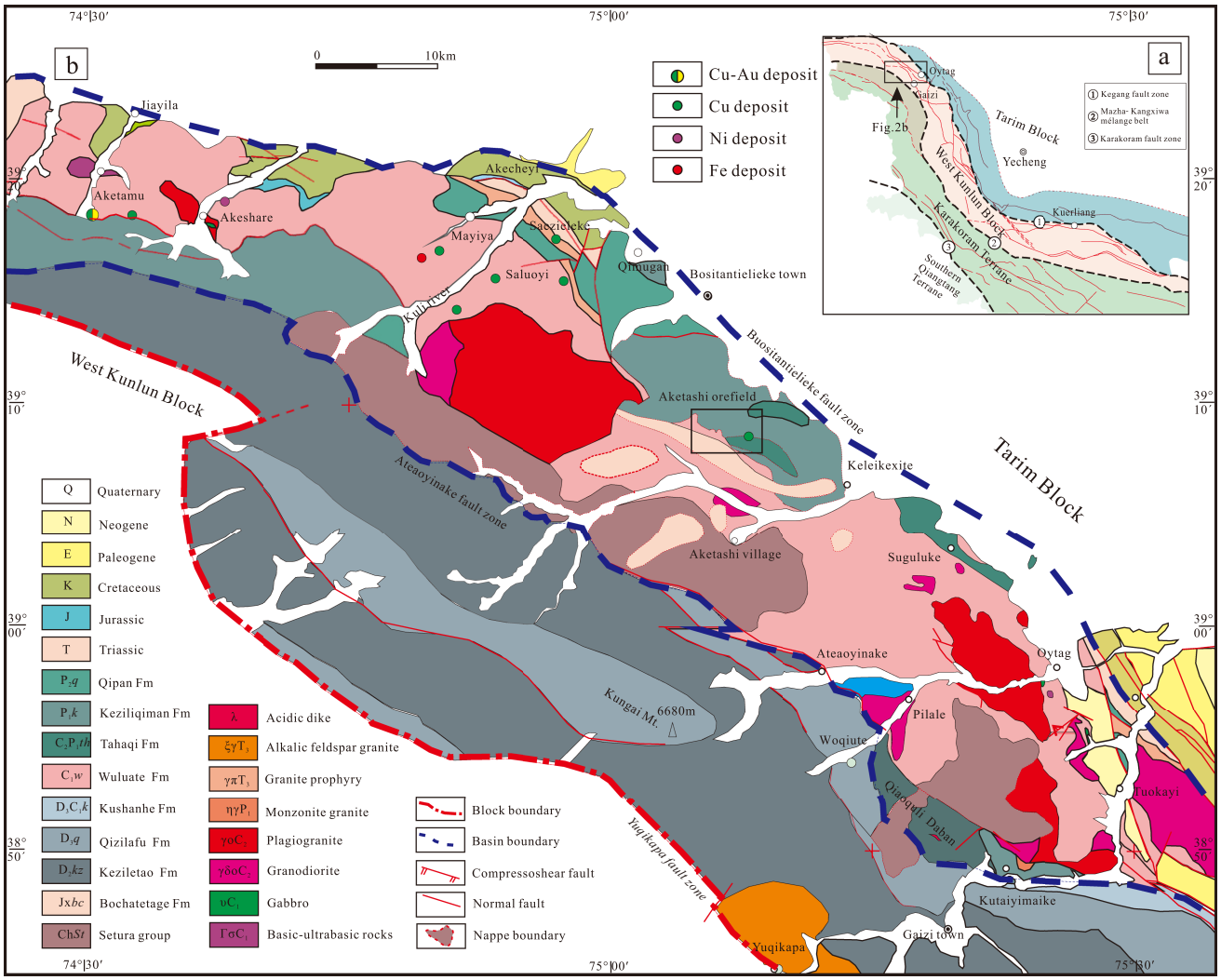

Fig. 2 Regional setting map showing the distribution area of metal deposits in the north slope of Kungai mountain

Chalcopyrite and sphalerite are interstitial, anhedral, and fine-grained (0.1–0.5 μm in diameter).

4 Sampling and analytical methods

In the Aketashi mining district, 19 pyrite ore samples of two types (laminated ore and massive ore) were collected. The samples were pre-cleaned with deionized water, dried at ambient temperature, pulverized using an agate shatter box, and sieved to a particle size of less than 200-mesh prior to chemical analysis. Total Hg (THg) concentrations and Hg isotopic composition were determined at the Institute of Geochemistry, Chinese Academy of Sciences, Guiyang, China. THg concentrations were determined using a DMA-80 Hg analyzer, which provided Hg recoveries of 90%–110% for the standard reference material GSS-4 (soil), with uncertainties of less than ±10% for triplicate sample analyses. Sample preparation for Hg isotope analysis followed the two-stage thermal combustion and pre-concentration method outlined by Zerkle et al. (2020). Both the standard reference material GSS-4 and procedural blanks were processed identically to the samples. The GSS-4 material resulted in Hg recoveries of 95%–100%, while the procedural blanks had Hg concentrations below detection limits. Pre-concentrated solutions were adjusted to a concentration of 0.5 ng mL^{-1} Hg in 10% HCl acid prior to analysis using a Neptune Plus multicollector inductively coupled plasma mass spectrometer (Yin et al. 2016b). Mercury isotopic measurements are reported in δ^{202}Hg notation, relative to the NIST-3133 Hg standard, in units of ‰:

$$\delta^{202}\mathrm{Hg}() = \left[\left(^{202}\mathrm{Hg}/^{198}\mathrm{Hg}\right)_{\mathrm{sample}}/\left(^{202}\mathrm{Hg}/^{198}\mathrm{Hg}\right)_{\mathrm{NIST3133}} - 1\right] \times 1000.$$

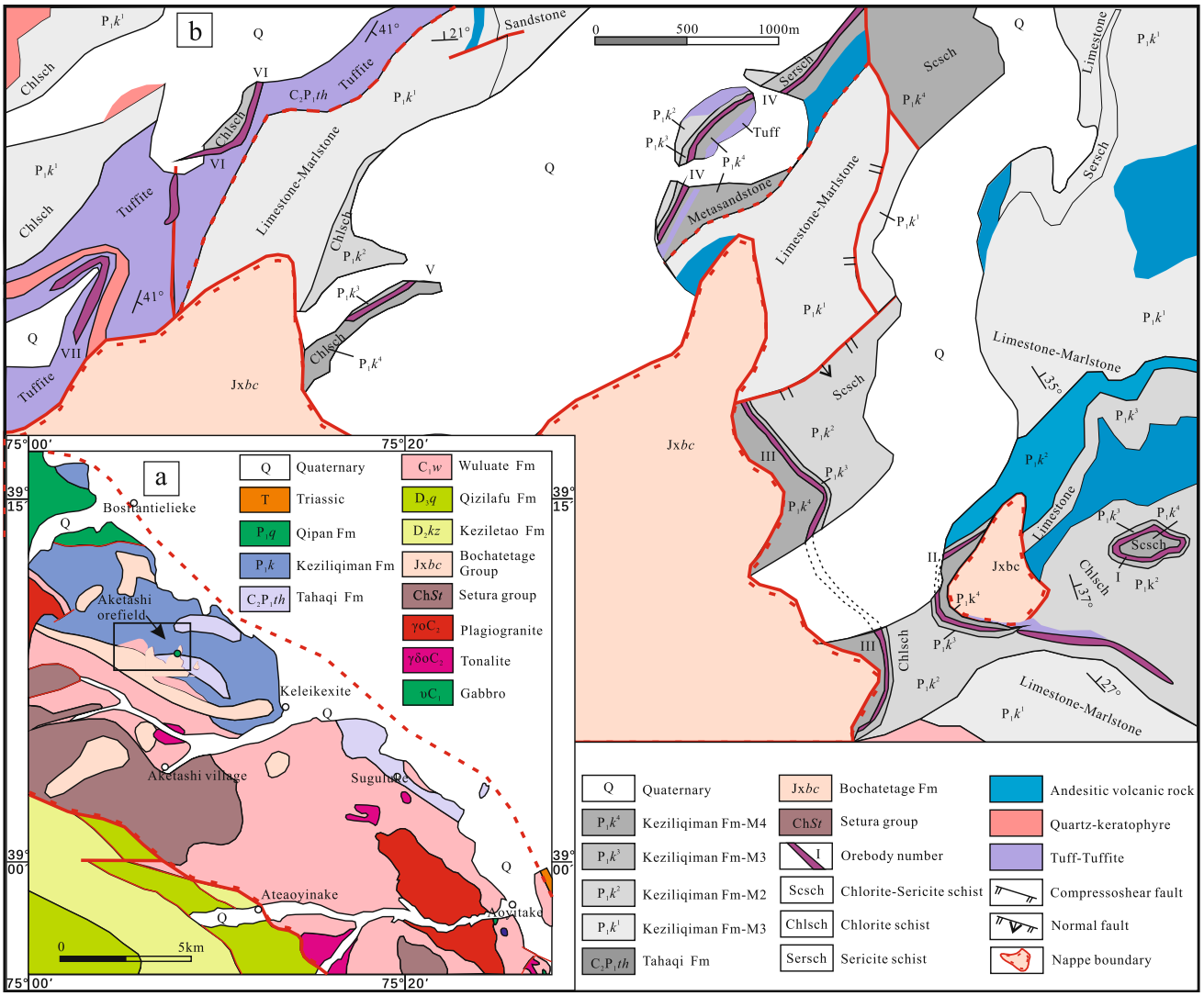

Fig. 3 **a** Geological map of the Aketashi region, showing locations of important VMS deposits. **b** Geological map of the Aketashi deposit

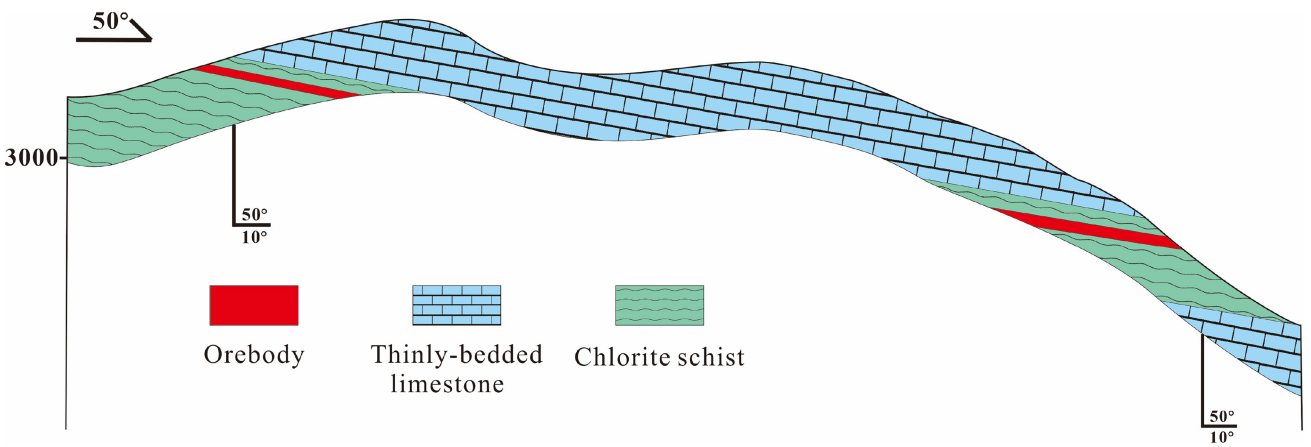

Fig. 4 Cross-section of the stratiform sulfide orebody in the Aketashi deposit, showing that the orebody is hosted in metavolcanic rocks

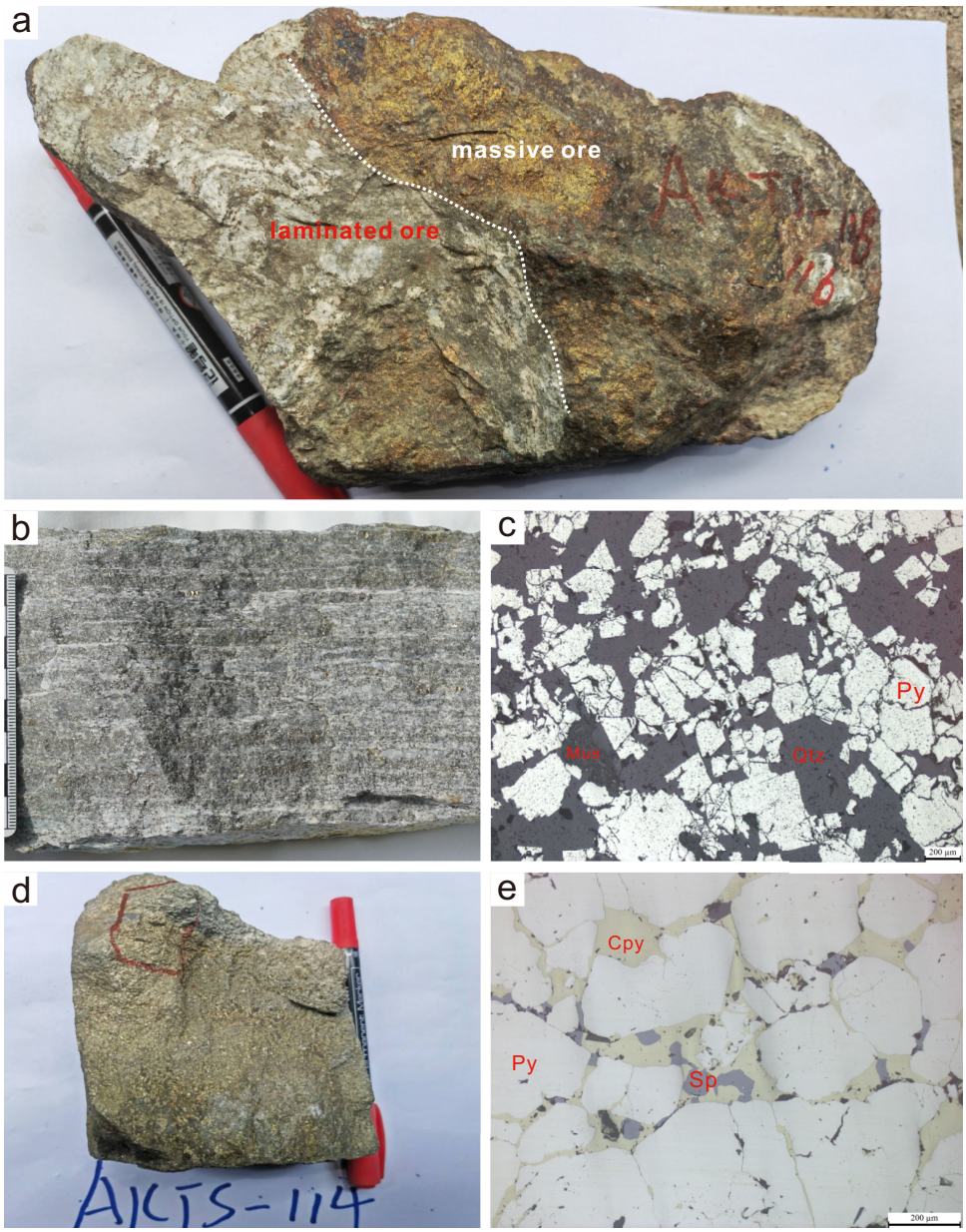

Fig. 5 General characteristics of the two main types of sulfide ores and the pyrites in them. **a** The laminated ore exhibits a texture that has been replaced and truncated by the massive ore, suggesting that its formation predates that of the massive ore. **b** Typical hand specimen of pyrite ores showing typical laminated and disseminated structures. **c** Reflection light photo of the pyrite ore, showing the pyrite and gangue minerals. **d** Typical hand specimen of Cu ores having massive structure. **e** Reflection light photo of the Cu ores showing its typical metal and mineral assemblages

MIF is reported in Δ notation, which describes the difference between the measured and theoretically predicted δ^{xxx}Hg value, in units of ‰:

$$\Delta^{xxx}\mathrm{Hg}(‰) = \delta^{xxx}\mathrm{Hg} - \beta \times \delta^{202}\mathrm{Hg},$$

where β is equal to 0.252 for ^{199}Hg, 0.502 for ^{200}Hg, 0.752 for ^{201}Hg, and 1.493 for ^{204}Hg (Blum and Bergquist 2007).

5 Results

In this study, 19 pyrite ore samples from two types (laminated and massive) collected from the Aketashi deposit were analyzed for their mercury content and mercury isotope composition. The results of the THg concentration and mercury isotope composition analyses are summarized in Table 1.

Pyrite samples of laminated ores from the Aketashi deposit have THg concentrations of 12.06 to 427.35 ppb, δ^{202}Hg values of −2.48 to −0.64‰, and Δ^{199}Hg values of −0.02‰ to 0.40‰. Pyrite samples of massive ores have THg concentrations of 29.43 to 427.35 ppb, δ^{202}Hg values of −2.35‰ to −0.87‰, and Δ^{199}Hg values of 0.00‰ to 0.26‰. Specifically, while the range of mercury content in both ore types is similar, the massive ore exhibits a notably higher average THg concentration of 151.64 ppb, compared to an average THg of 92.89 ppb in the laminated ores.

Table 1 Hg content and Hg isotope data for pyrite ores in the Aketashi deposit

Sample	Lithology	Hg ppm	δ^{199}Hg ‰	δ^{200}Hg ‰	δ^{201}Hg ‰	δ^{202}Hg ‰	Δ^{199}Hg ‰	Δ^{200}Hg ‰	Δ^{201}Hg ‰
AKTS-101	Laminated ore	427.35	−0.23	−1.23	−1.53	−2.48	0.40	0.02	0.33
AKTS-102		41.38	−0.28	−0.64	−0.89	−1.25	0.04	−0.01	0.05
AKTS-103		151.82	0.01	−0.27	−0.32	−0.64	0.17	0.05	0.15
AKTS-107		47.48	−0.20	−0.44	−0.49	−0.70	−0.02	−0.09	0.03
AKTS-108		37.53	−0.27	−0.67	−0.84	−1.20	0.03	−0.07	0.06
AKTS-109		52.98	−0.12	−0.40	−0.50	−0.78	0.08	−0.01	0.09
AKTS-112		12.06	−0.22	−0.59	−0.80	−1.13	0.07	−0.02	0.05
AKTS-113		32.78	−0.40	−0.97	−1.34	−1.76	0.04	−0.08	−0.02
AKTS-115		32.59	−0.29	−0.71	−0.98	−1.36	0.05	−0.03	0.04
AKTS-106–3	Massive ore	53.70	−0.12	−0.31	−0.37	−0.63	0.04	0.01	0.10
AKTS-110–1		141.40	−0.11	−0.52	−0.67	−1.03	0.15	0.00	0.10
AKTS-110–2		98.02	−0.06	−0.47	−0.52	−0.91	0.17	−0.02	0.16
AKTS-122		382.65	−0.15	−0.62	−0.84	−1.38	0.20	0.07	0.19
AKTS-124		32.78	−0.22	−0.72	−0.90	−1.38	0.13	−0.02	0.14
AKTS-125		47.76	−0.33	−1.15	−1.55	−2.35	0.26	0.03	0.22
AKTS-126		427.35	0.22	0.46	0.67	0.87	0.00	0.03	0.02
AKTS-127		150.60	0.09	−0.14	−0.12	−0.48	0.21	0.10	0.24
AKTS-128		152.71	0.07	0.05	0.19	0.05	0.06	0.02	0.15
AKTS-130–2		29.43	−0.35	−0.76	−1.03	−1.52	0.03	0.00	0.11

Nevertheless, no substantial variations were observed in the mercury isotope composition of the two ore types. Therefore, in subsequent discussions, the two ore types will not be distinguished.

Among the 19 analyzed samples, 18 exhibited positive Δ^{199}Hg values (up to 0.40‰), while one sample showed a slightly negative value (−0.02‰).

Two regression lines with slopes of 1.17 and 1.13 were derived from the Δ^{199}Hg and Δ^{201}Hg values of these samples, indicating Δ^{199}Hg/Δ^{201}Hg ratios of 1.17 and 1.13. These ratios are consistent with those observed during the photochemical reduction of Hg(II) in water (Δ^{199}Hg/Δ^{201}Hg = 1.0–1.3) (Bergquist and Blum 2007; Zheng and Hintelmann 2009), suggesting that the Hg MIF in the samples originated from a photochemical reaction.

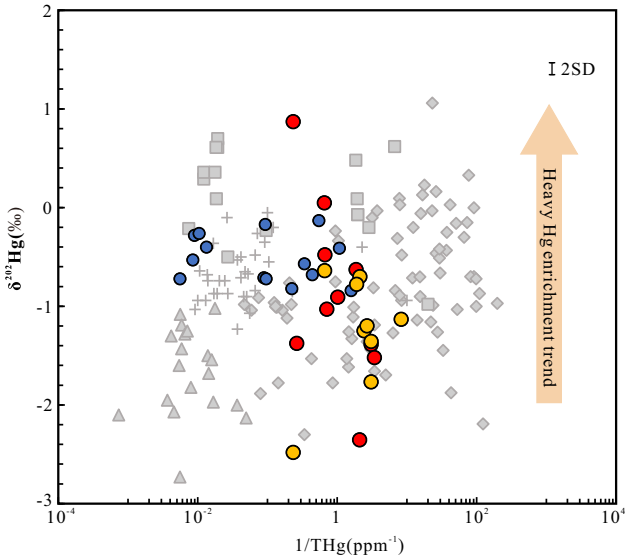

Fig. 6 Plot of Δ^{199}Hg vs. δ^{202}Hg for the studied samples. The field for terrestrial Hg is from Blum et al. (2014) and references therein, and the field for marine sedimentary Hg is from Yin et al. (2015) and Meng et al. (2019)

6 Discussion

6.1 Enrichment of light Hg isotopes in the Aketashi deposit

The δ^{202}Hg values of pyrite ores from the Aketashi deposit range from −2.48‰ to 0.87‰ (Fig. 6; mean = −1.05‰), which are significantly lower than those of both marine/terrestrial reservoirs (generally negative δ^{202}Hg; Blum et al. 2014) and mantle-derived materials (near-zero δ^{202}Hg; Sherman et al. 2009). This pronouncedly light Hg isotope enrichment (Fig. 6) strongly suggests mercury mass-dependent fractionation (MDF) during hydrothermal processes. We attribute this fractionation to high-temperature reducing conditions in the magmatic-hydrothermal system, which promote (1) Hg^0 volatilization (preferentially releasing lighter isotopes such as ^{200}Hg) and (2) retention of heavier isotopes (e.g., ^{202}Hg) in residual sulfides (Smith et al. 2005,

2008; Sherman et al. 2009). These mechanisms align with isotopic behaviors observed in other magmatic-hydrothermal systems, where boiling, redox fluctuations, and sulfide precipitation drive Hg–MDF (Zheng et al. 2007). The correlation between low δ^{202}Hg values and magmatic-hydrothermal activity underscores the utility of Hg isotopes in distinguishing fluid evolution pathways in VMS systems.

6.2 Hg isotopic MIF constraints on the source of ore-forming fluid in the Aketashi deposit

Mass-independent fractionation (MIF) of mercury isotopes (Δ^{199}Hg and Δ^{201}Hg) serves as a critical tracer for distinguishing mercury sources in hydrothermal systems, as hydrothermal processes typically induce negligible Hg–MIF (Xu et al. 2018; Yin et al. 2016a). Mercury MIF arises from two principal mechanisms: (1) the nuclear volume effect (NVE), dominant during Hg^0 evaporation and dark Hg(II) reduction, producing Δ^{199}Hg/Δ^{201}Hg ratios of ~1.6–1.7 (Estrade et al. 2009; Ghosh et al. 2013; Zheng and Hintelmann 2010); and (2) the magnetic isotope effect (MIE), associated with photochemical processes such as aqueous Hg(II) photoreduction and methylmercury (MeHg) photodegradation, yielding Δ^{199}Hg/Δ^{201}Hg ratios of ~1.0 and ~1.3, respectively (Bergquist and Blum 2007; Zheng and Hintelmann 2009).

Pronounced Hg–MIF signals (Δ^{199}Hg up to ~10‰) are predominantly observed in Earth's surface environments (e.g., atmosphere, rainwater, aquatic biota), where photochemical Hg(II) reduction dominates (Blum et al. 2014; Sonke 2011). In contrast, the primitive mantle and the asthenospheric mantle exhibit near-zero Δ^{199}Hg values (0.00‰ ± 0.10‰, 2SD; Moynier et al. 2021; Deng et al. 2022a), reflecting minimal MIF in deep-Earth reservoirs (Sherman et al. 2009; Smith et al. 2008). Significant Hg–MIF in some hydrothermal sulfide deposits has been attributed to epigenetic Hg inheritance via sedimentation and hydrothermal leaching. Notably, recent studies have demonstrated that low-temperature hydrothermal ore deposits (such as Au, Sb, Pb, and Zn deposits) formed in volcanic-arc and intracontinental settings display distinct Δ^{199}Hg signatures (Δ^{199}Hg > 0 in arc settings; Δ^{199}Hg < 0 in intracontinental settings), indicating that their metallogenic materials originate from marine and terrestrial environments, respectively (Gray et al. 2013; Deng et al. 2021b, 2022b).

The Aketashi pyrite samples exhibit a positive correlation between Δ^{199}Hg and Δ^{201}Hg (Δ^{199}Hg/Δ^{201}Hg = 1.13 and 1.17, Fig. 7). This suggests that some of the Hg–MIF in the Aketashi deposit was caused by the Hg(II) photoreduction before precipitation into pyrites. Some pyrite samples from the Aketashi deposit exhibit obvious positive Δ^{199}Hg values (> 0.1‰, n = 9; Fig. 8), overlapping with values reported for modern seawater (0.21 ± 0.13; Strok et al. 2015) and marine

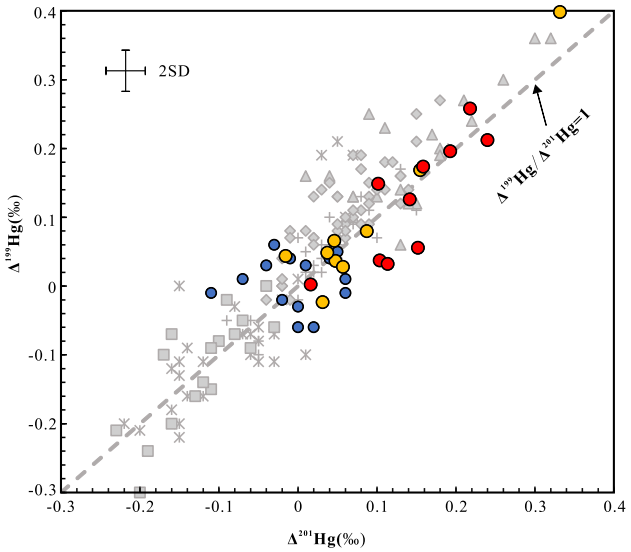

Fig. 7 Plots of δ^{202}Hg versus 1/THg for the studied samples and compiled data. The sample symbols and data sources are the same as in Fig. 5

sediments (0.14‰ ± 0.18‰; Gehrke et al. 2009; Meng et al. 2019; Yin et al. 2015). This suggests a substantial contribution of submarine Hg (seawater or seafloor sediments) to the deposit. However, the majority of samples from Aketashi have Δ^{199}Hg values within 0‰ ± 0.1‰, implicating a potential contribution from magmatic or mantle-derived fluids. The Aketashi Δ^{199}Hg values closely resemble those of Chinese VMS (Yin et al. 2016a) and sediment-hosted stratiform sulfide (SHSS) deposits (e.g., Xiangquan Tl deposit; Meng et al. 2024), all of which mirror marine reservoirs (Fig. 8). This consistency implies shared Hg sources among these deposits. In contrast, negative Δ^{199}Hg values in sediment-hosted Pb–Zn and stratiform ironstone deposits (Fig. 9; Xu et al. 2018; Zhou et al. 2024) highlight distinct metallogenic mechanisms for the Aketashi system.

Small but significant Hg–MIF (Δ^{199}Hg: −0.02‰ to 0.40‰) and exceptionally low δ^{202}Hg values (−2.48‰ to 0.87‰) of the Aketashi pyrites reflect a unique interplay of seawater and magmatic hydrothermal fluids. During the Late Paleozoic, the Paleo-Tethys convergence facilitated the development of the Oytag-Kuerliang back-arc basin in the Western Kunlun region (Li et al. 2007; Liu et al. 2014a; Zhang et al. 2021). In this extensional setting, seafloor volcanism and rifting provided conduits for ascending mantle-derived or lower-crustal fluids enriched in Cu and Zn, while contemporaneous seawater circulation contributed photochemically altered Hg. This dual-fluid model reconciles the observed Hg–MIF signals with the strong Hg–MDF recorded in δ^{202}Hg, underscoring the complex hybridization of deep and surface reservoirs in VMS mineralization.

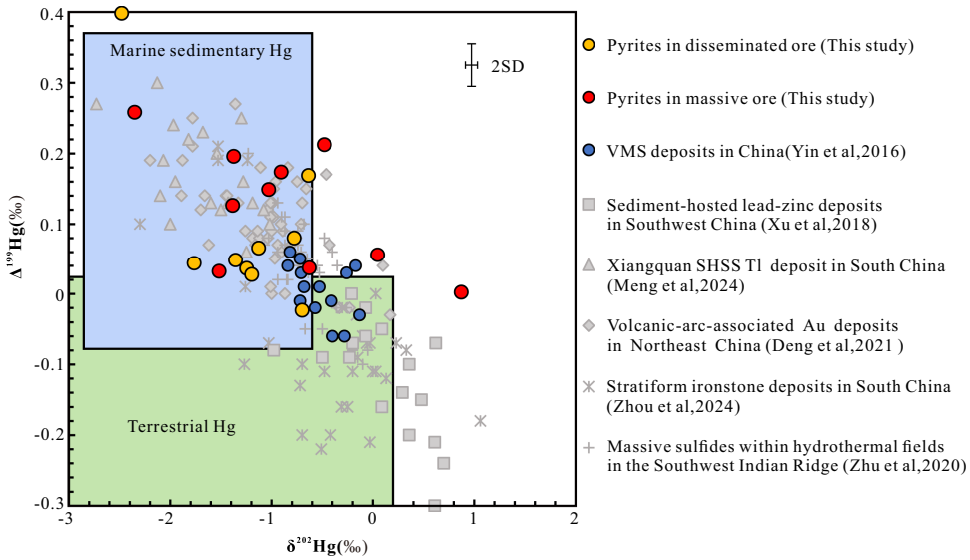

Fig. 8 Plots of Δ^{199}Hg versus 1/THg for the studied samples and compiled data. The sample symbols and data sources are the same as in Fig. 5

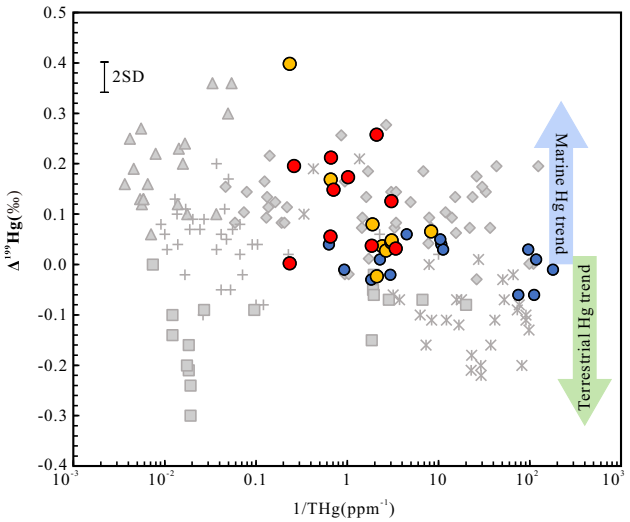

Fig. 9 Plot of Δ^{199}Hg versus Δ^{201}Hg for the studied samples. The sample symbols and data sources are the same as in Fig. 5

6.3 Implications for the sources of hydrothermal fluid in VMS deposits

The origins of hydrothermal fluids in VMS deposits have long been a subject of intense scientific debate. Distinguishing between the contributions of magmatic and seawater-derived fluids continues to be a fundamental challenge in elucidating the genesis of these deposits. In this context, Hg isotopes serve as a robust tracer. For instance, VMS deposits associated with arc magmatism typically display positive Δ^{199}Hg values, indicative of a predominant seawater influence, while other deposits formed in intracontinental settings exhibit more negative values, suggesting a greater contribution from magmatic or crustal fluids (Deng et al. 2021a; Yin et al. 2019). These findings demonstrate that Hg isotopes serve as an effective tracer for identifying the sources of hydrothermal fluids in VMS systems. Furthermore, the integration of Hg isotope data with trace element signatures or other isotopic characteristics (such as Sb, Sn, and Cu; Mason et al. 2016; Powell et al. 2017; Zhai et al. 2021) in the future can provide a robust and reliable methodology for elucidating the intricate interactions among magmatic, crustal, and seawater-derived fluids during the formation of VMS deposits (Blum et al. 2014; Deng et al. 2021b; Yin et al. 2016a). This approach holds considerable promise for future research endeavors focused on unraveling the genesis and fluid dynamics of VMS systems (Barrie and Hannington 1997; Large et al. 2001).

7 Conclusion

The Aketashi VMS deposit exhibits significant Hg isotope variations, characterized by exceptionally negative δ^{202}Hg values and small but significant positive positive Δ^{199}Hg values. These isotopic signatures suggest that the deposit's Hg originated from a mix of seawater and magmatic/mantle fluids, highlighting the role of hydrothermal processes in Hg enrichment. The findings indicate that Hg isotopes are effective tracers for identifying fluid sources in VMS deposits and provide critical insights into the mineralization mechanisms. Our model links Late Paleozoic back-arc tectonics to enhanced seawater infiltration, providing a framework for reinterpreting VMS genesis in similar settings.

Acknowledgements We acknowledge the financial supports of the Strategic Priority Research Program of the Chinese Academy of Sciences (Grant No. XDA0430201) and the National Natural Science Foundation of China (NSFC Nos. U1603245, U1703242, and U1812402). We are also grateful to the assistance of Profs. Runsheng Yin, Changzhou Deng, and Dr. Xueyun Wang, and Di Chen during the preparation and analyses of Hg isotopes.

Author contributions Ziru Jin: Writing—original draft, Formal analysis, Investigation, Methodology; Zhengwei Zhang: Funding acquisition, Supervision, Conceptualization; Chengquan Wu: Conceptualization, Writing—review & editing; Jinhong Xu: Data curation, Investigation; Xiyao Li: Data curation, Investigation.

Funding Innovative Research Group Project of the National Natural Science Foundation of China (NSFC Nos. U1603245, U1703242, U1812402).

Declarations

Conflict of interest This manuscript has not been published or presented elsewhere in part or in entirety, and it is not under consideration by another journal. All the authors have approved the manuscript and agree with submission to the esteemed journal. There are no conflicts of interest to declare.

References

Barrie CT, Hannington MD (1997) Classification of volcanic-associated massive sulfide deposits based on host-rock composition. Rev Econ Geol 8:1–11

Bergquist BA, Blum JD (2007) Mass-dependent and-independent fractionation of Hg isotopes by photoreduction in aquatic systems. Science 318(5849):417–420. https://doi.org/10.1126/science.1148050

Blum JD, Bergquist BA (2007) Reporting of variations in the natural isotopic composition of mercury. Anal Bioanal Chem 388(2):353–359. https://doi.org/10.1007/s00216-007-1236-9

Blum JD, Sherman LS, Johnson MW (2014) Mercury isotopes in Earth and environmental sciences. Annu Rev Earth Planet Sci 42:249–269. https://doi.org/10.1146/annurev-earth-050212-124107

Cui JT, Bian XW, Wang GB (2006) Geological composition and evolution of the western Qunlun. Geol Shaanxi 24(1):1–11

Deng CZ, Li CL, Rong YM, Chen D, Zhou T, Wang XY, Chen HY, Lehmann B, Yin RS (2021a) Different metal sources in the evolution of an epithermal ore system: evidence from mercury isotopes associated with the Erdaokan epithermal Ag–Pb–Zn deposit, NE China. Gondwana Res 95:1–9. https://doi.org/10.1016/j.gr.2021.03.010

Deng CZ, Sun GY, Rong YM, Sun RY, Sun DY, Lehmann B, Yin RS (2021b) Recycling of mercury from the atmosphere-ocean system into volcanic-arc–associated epithermal gold systems. Geology 49(3):309–313. https://doi.org/10.1130/g48132.1

Deng CZ, Gou J, Sun DY, Sun GY, Tian ZD, Lehmann B, Moynier F, Yin RS (2022a) Mercury isotopic composition of igneous rocks from an accretionary orogen: implications for lithospheric recycling. Geology 50(9):1001–1006. https://doi.org/10.1130/g50131.1

Deng CZ, Lehmann B, Xiao TT, Tan QP, Chen D, Tian ZD, Wang XY, Sun GY, Yin RS (2022b) Intracontinental and arc-related hydrothermal systems display distinct δ^{202}Hg and Δ^{199}Hg features: implication for large-scale mercury recycling and isotopic fractionation in different tectonic settings. Earth Planet Sci Lett 593:117646. https://doi.org/10.1016/j.epsl.2022.117646

Estrade N, Carignan J, Sonke JE, Donard OFX (2009) Mercury isotope fractionation during liquid–vapor evaporation experiments. Geochim Cosmochim Acta 73(10):2693–2711. https://doi.org/10.1016/j.gca.2009.01.024

Fu SL, Hu RZ, Yin RS, Yan J, Mi XF, Song ZC, Sullivan NA (2020) Mercury and in situ sulfur isotopes as constraints on the metal and sulfur sources for the world's largest Sb deposit at Xikuangshan, Southern China. Miner Depos 55(7):1353–1364. https://doi.org/10.1007/s00126-019-00940-1

Gehrke GE, Blum JD, Meyers PA (2009) The geochemical behavior and isotopic composition of Hg in a mid-Pleistocene western Mediterranean sapropel. Geochim Cosmochim Acta 73(6):1651–1665. https://doi.org/10.1016/j.gca.2008.12.012

Ghosh S, Schauble EA, Lacrampe Couloume G, Blum JD, Bergquist BA (2013) Estimation of nuclear volume dependent fractionation of mercury isotopes in equilibrium liquid–vapor evaporation experiments. Chem Geol 336:5–12. https://doi.org/10.1016/j.chemgeo.2012.01.008

Grasby SE, Shen WJ, Yin RS, Gleason JD, Blum JD, Lepak RF, Hurley JP, Beauchamp B (2017) Isotopic signatures of mercury contamination in latest Permian oceans. Geology 45(1):55–58. https://doi.org/10.1130/g38487.1

Gray JE, Pribil MJ, Higueras PL (2013) Mercury isotope fractionation during ore retorting in the Almadén mining district, Spain. Chem Geol 357:150–157. https://doi.org/10.1016/j.chemgeo.2013.08.036

Hannington MD (2014) Volcanogenic massive sulfide deposits. Treatise Geochem 47(5):463–488. https://doi.org/10.1016/b978-0-08-095975-7.01120-7

Hannington M, Herzig PM, Scott SD (2005) Seafloor massive sulfide deposits: evolution of a submarine magmatic-hydrothermal system. Econ Geol 100:1097–1133

Jia QZ, Li WM, Yu PS, Wu JR, Zhang DS, Gao P, Chen GM (1999) Metallogenic conditions and metallogenic prediction of massive sulfide deposits in west Kunlun. Geology Press, Beijing

Large RR, Lydon JW, Barrie CT (2001) Volcanogenic massive sulfide deposits. In: Economic geology: one hundredth anniversary, pp 561–607

Li BQ, Yao JX, Ji WH, Zhang JL, Yin ZY, Chen GC, Nin XW, Zhang QS, Kong WN, Wang F, Liu XP (2006) Characteristics and zircon SHRIMP U-Pb ages of the arc magmatic rocks in Mazar, southern Yecheng, West Kunlun Mountains. Geol Bull China 25(1–2):124–132

Li BQ, Ji WH, Bian XW, Wang F, Li W (2007) The composition and geological significance of the Mazha tectonic Melange in west Kunlun Mountains. Geoscience 21(1):78–86. https://doi.org/10.3969/j.issn.1000-8527.2007.01.009

Liu KF, Wang YH, Jiang GL, Zhang SM, Zhang KX (2014a) Evolution of Neoproterozoic-Mesozoic sedimentary basins of west Kunlun area. Editor Comm Earth Sci J China Univ Geosci 8:987–999. https://doi.org/10.3799/dqkx.2014.090

Liu Z, Jiang YH, Jia RY, Zhao P, Zhou Q, Wang GC, Ni CY (2014b) Origin of Middle Cambrian and Late Silurian potassic granitoids from the western Kunlun orogen, northwest China: a magmatic response to the Proto-Tethys evolution. Mineral Petrol 108(1):91–110. https://doi.org/10.1007/s00710-013-0288-0

Liu YF, Qi HW, Bi XW, Hu RZ, Qi LK, Yin RS, Tang YY (2021) Mercury and sulfur isotopic composition of sulfides from sediment-hosted lead-zinc deposits in Lanping basin, Southwestern

China. Chem Geol 559:119910. https://doi.org/10.1016/j.chemgeo.2020.119910
Mason AH, Powell WG, Bankoff HA, Mathur R, Bulatović A, Filipović V, Ruiz J (2016) Tin isotope characterization of bronze artifacts of the central Balkans. J Archaeol Sci 69:110–117. https://doi.org/10.1016/j.jas.2016.04.012
Mattern F, Schneider W (2000) Suturing of the proto- and paleo-Tethys oceans in the western Kunlun (Xinjiang, China). J Asian Earth Sci 18(6):637–650. https://doi.org/10.1016/S1367-9120(00)00011-0
Meier MMM, Cloquet C, Marty B (2016) Mercury (Hg) in meteorites: variations in abundance, thermal release profile, mass-dependent and mass-independent isotopic fractionation. Geochim Cosmochim Acta 182:55–72. https://doi.org/10.1016/j.gca.2016.03.007
Meng M, Sun RY, Liu HW, Yu B, Yin YG, Hu LG, Shi JB, Jiang GB (2019) An integrated model for input and migration of mercury in Chinese coastal sediments. Environ Sci Technol 53(5):2460–2471. https://doi.org/10.1021/acs.est.8b06329
Meng L, Zhou MF, Chen WT (2024) Using Hg isotopes and trace elements to constrain the origin of the Ordovician Xiangquan Tl deposit, South China. J Asian Earth Sci 268:106168. https://doi.org/10.1016/j.jseaes.2024.106168
Moynier F, Jackson MG, Zhang K, Cai HM, Halldórsson SA, Pik R, Day JMD, Chen JB (2021) The mercury isotopic composition of Earth's mantle and the use of mass independently fractionated Hg to test for recycled crust. Geophys Res Lett 48(17):e2021GL094301. https://doi.org/10.1029/2021gl094301
Mu SL (2016) Volcanic rocks tectonic environments and metallogenesis of typical mineral deposits in Kungai mountains, West Kunlun. The University of Chinese Academy of Sciences, Beijing
Pan YS (1990) Tectonic features and evolution of the western Kunlun Mountain region. Chin J Geolo 25(03):224–232
Powell W, Mathur R, Bankoff HA, Mason A, Bulatović A, Filipović V, Godfrey L (2017) Digging deeper: Insights into metallurgical transitions in European prehistory through copper isotopes. J Archaeol Sci 88:37–46. https://doi.org/10.1016/j.jas.2017.06.012
Rytuba JJ (2003) Mercury from mineral deposits and potential environmental impact. Environ Geol 43(3):326–338. https://doi.org/10.1007/s00254-002-0629-5
Shen J, Algeo TJ, Planavsky NJ, Yu JX, Feng QL, Song HJ, Song HY, Rowe H, Zhou L, Chen JB (2019) Mercury enrichments provide evidence of early Triassic volcanism following the end-Permian mass extinction. Earth Sci Rev 195:191–212. https://doi.org/10.1016/j.earscirev.2019.05.010
Sherman LS, Blum JD, Nordstrom DK, McCleskey RB, Barkay T, Vetriani C (2009) Mercury isotopic composition of hydrothermal systems in the Yellowstone Plateau volcanic field and Guaymas Basin sea-floor rift. Earth Planet Sci Lett 279(1–2):86–96. https://doi.org/10.1016/j.epsl.2008.12.032
Smith CN, Kesler SE, Klaue B, Blum JD (2005) Mercury isotope fractionation in fossil hydrothermal systems. Geology 33(10):825. https://doi.org/10.1130/g21863.1
Smith CN, Kesler SE, Blum JD, Rytuba JJ (2008) Isotope geochemistry of mercury in source rocks, mineral deposits and spring deposits of the California Coast Ranges, USA. Earth Planet Sci Lett 269(3–4):399–407. https://doi.org/10.1016/j.epsl.2008.02.029
Song Z, Li HM, Li LX, Ding JH, Meng J (2021) Iron isotopes and trace element compositions of magnetite from the submarine volcanic-hosted iron deposits in east Tianshan, NW China: new insights into the mineralization processes. J Earth Sci 32(1):219–234. https://doi.org/10.1007/s12583-020-1060-0
Sonke JE (2011) A global model of mass independent mercury stable isotope fractionation. Geochim Cosmochim Acta 75(16):4577–4590. https://doi.org/10.1016/j.gca.2011.05.027
Štrok M, Baya PA, Hintelmann H (2015) The mercury isotope composition of Arctic coastal seawater. C R Geosci 347(7–8):368–376. https://doi.org/10.1016/j.crte.2015.04.001
Sun HT (2003) An introduction to the metallogenic province of West Kunlun. Geology Press, Beijing
Thibodeau AM, Ritterbush K, Yager JA, West AJ, Ibarra Y, Bottjer DJ, Berelson WM, Bergquist BA, Corsetti FA (2016) Mercury anomalies and the timing of biotic recovery following the end-Triassic mass extinction. Nat Commun 7:11147. https://doi.org/10.1038/ncomms11147
Varekamp JC, Buseck PR (1984) The speciation of mercury in hydrothermal systems, with applications to ore deposition. Geochim Cosmochim Acta 48(1):177–185. https://doi.org/10.1016/0016-7037(84)90359-4
Wang CM, Deng J, Zhang ST, Yang LQ (2010) Metallogenic province and large scale mineralization of volcanogenic massive sulfide deposits in China. Resour Geol 60(4):404–413. https://doi.org/10.1111/j.1751-3928.2010.00127.x
Wang QF, Zhao HS, Yang L, Groves DI, Han JL, Qiu KF, Li DP, Liu Z, Zhao R, Deng J (2025) Formation of the giant Cretaceous Jiaodong-type orogenic gold province of the North China Craton: a consequence of lithospheric multi-layer reworking. Geosci Front 16(3):102047. https://doi.org/10.1016/j.gsf.2025.102047
Xiao WJ, Windley BF, Liu DY, Jian P, Liu CZ, Yuan C, Sun M (2005) Accretionary tectonics of the western Kunlun Orogen, China: a Paleozoic-early Mesozoic, long-lived active continental margin with implications for the growth of southern Eurasia. J Geol 113(6):687–705. https://doi.org/10.1086/449326
Xu CX, Yin RS, Peng JT, Hurley JP, Lepak RF, Gao JF, Feng XB, Hu RZ, Bi XW (2018) Mercury isotope constraints on the source for sediment-hosted lead-zinc deposits in the Changdu area, southwestern China. Miner Depos 53(3):339–352. https://doi.org/10.1007/s00126-017-0743-7
Xu CX, Meng YM, Huang C, Tang C, Zheng FW (2021) Advances in the study on mercury isotope geochemistry and its application in mineral deposits. Rock Mineral Anal 2:173–186. https://doi.org/10.15898/j.cnki.11-2131/td.202009210125
Yin A, Harrison TM (2000) Geologic evolution of the Himalayan-Tibetan orogen. Annu Rev Earth Planet Sci 28:211–280. https://doi.org/10.1146/annurev.earth.28.1.211
Yin RS, Feng XB, Chen BW, Zhang JJ, Wang WX, Li XD (2015) Identifying the sources and processes of mercury in subtropical estuarine and ocean sediments using Hg isotopic composition. Environ Sci Technol 49(3):1347–1355. https://doi.org/10.1021/es504070y
Yin RS, Feng XB, Hurley JP, Krabbenhoft DP, Lepak RF, Hu RZ, Zhang Q, Li ZG, Bi XW (2016a) Mercury isotopes as proxies to identify sources and environmental impacts of mercury in sphalerites. Sci Rep 6:18686. https://doi.org/10.1038/srep18686
Yin RS, Krabbenhoft DP, Bergquist BA, Zheng W, Lepak RF, Hurley JP (2016b) Effects of mercury and thallium concentrations on high precision determination of mercury isotopic composition by Neptune Plus multiple collector inductively coupled plasma mass spectrometry. J Anal at Spectrom 31(10):2060–2068. https://doi.org/10.1039/C6JA00107F
Yin RS, Deng CZ, Lehmann B, Sun GY, Lepak RF, Hurley JP, Zhao CH, Xu GW, Tan QP, Xie ZJ, Hu RZ (2019) Magmatic-hydrothermal origin of mercury in carlin-style and epithermal gold deposits in China: evidence from mercury stable isotopes. ACS Earth Space Chem 3(8):1631–1639. https://doi.org/10.1021/acsearthspacechem.9b00111
Zerkle AL, Yin RS, Chen CY, Li XD, Izon GJ, Grasby SE (2020) Anomalous fractionation of mercury isotopes in the late Archean atmosphere. Nat Commun 11(1):1709. https://doi.org/10.1038/s41467-020-15495-3
Zhai DG, Liu JJ, Wang JP, Yao MJ, Wu SH, Fu C, Liu ZJ, Wang SG, Li YX (2013) Fluid evolution of the Jiawula Ag–Pb–Zn deposit, Inner Mongolia: mineralogical, fluid inclusion, and stable isotopic

evidence. Int Geol Rev 55(2):204–224. https://doi.org/10.1080/00206814.2012.692905

Zhai DG, Mathur R, Liu SG, Liu JJ, Godfrey L, Wang KX, Xu JW, Vervoort J (2021) Antimony isotope fractionation in hydrothermal systems. Geochim Cosmochim Acta 306:84–97. https://doi.org/10.1016/j.gca.2021.05.031

Zhang CL, Li XH, Li ZX, Lu SN, Ye HM, Li HM (2007) Neoproterozoic ultramafic–mafic-carbonatite complex and granitoids in Quruqtagh of northeastern Tarim Block, western China: geochronology, geochemistry and tectonic implications. Precambrian Res 152(3–4):149–169. https://doi.org/10.1016/j.precamres.2006.11.003

Zhang ZW, Yang XY, Zhang LC, Wu CQ, Luo TY, Zhu WG, Xu JH, Hu PC, Li XY, Jin ZR (2021) Sedimentation and mineralization of the late Paleozoic extensional basin in the western Kunlun Mountains, China. Solid Earth Sci 6(2):142–177. https://doi.org/10.1016/j.sesci.2021.02.001

Zhang YJ, Li XY, Wu CQ, Xu JH, Zhang ZW (2024) Evolution and mineralization of the Late Paleozoic Basin in the west Kunlun. China Kwxb 44(4):478–492. https://doi.org/10.3724/j.1000-4734.2024.44.024

Zhang LD, Deng CZ, Tang Y, Ni XR, Yang BZ, Liang SS, Liu WP, Ding JS, Zeng XH (2025) Pyrite geochemistry and S–Hg isotopes reveal the ore genesis of the hydrothermal vein-type Cuiluan Ag–Pb–Zn deposit in NE China. J Earth Sci. https://doi.org/10.1007/s12583-025-0201-x

Zhao G, Zhai DG, Liu JJ, Mathur R (2023) Fluid inclusion and H–O–S–Pb isotope constraints on the origin of carbonate-hosted Hg–Sb mineralization at Gongguan, Central China. Miner Depos 58(8):1519–1536. https://doi.org/10.1007/s00126-023-01192-w

Zheng W, Hintelmann H (2009) Mercury isotope fractionation during photoreduction in natural water is controlled by its Hg/DOC ratio. Geochim Cosmochim Acta 73(22):6704–6715. https://doi.org/10.1016/j.gca.2009.08.016

Zheng W, Hintelmann H (2010) Nuclear field shift effect in isotope fractionation of mercury during abiotic reduction in the absence of light. J Phys Chem A 114(12):4238–4245. https://doi.org/10.1021/jp910353y

Zheng W, Foucher D, Hintelmann H (2007) Mercury isotope fractionation during volatilization of Hg(0) from solution into the gas phase. J Anal at Spectrom 22(9):1097–1104. https://doi.org/10.1039/B705677J

Zhou MF, Jonathan Lyu Y, Ray Liu Z, Liu PP, Meng L, Johnson Qiu W, Winston Zhao W (2024) Devonian stratiform ironstone deposits in South China formed in a shallow marine environment of a passive continental margin. J Asian Earth Sci 262:105997. https://doi.org/10.1016/j.jseaes.2023.105997